Liquid Phase Sintering of Boron-Containing Powder Metallurgy Steel with Chromium and Carbon

MING-WEI WU, YU-CHI FAN, HER-YUEH HUANG, and WEN-ZHANG CAI

Liquid phase sintering is an effective method to improve the densification of powder metallurgy materials. Boron is an excellent alloying element for liquid phase sintering of Fe-based materials. However, the roles of chromium and carbon, and particularly that of the former, on liquid phase sintering are still undetermined. This study demonstrated the effects of chromium and carbon on the microstructure, elemental distribution, boride structure, liquid formation, and densification of Fe-B-Cr and Fe-B-Cr-C steels during liquid phase sintering. The results showed that steels with 0.5 wt pct C densify faster than those without 0.5 wt pct C. Moreover, although only one liquid phase forms in Fe-B-Cr steel, adding 0.5 wt pct C reduces the formation temperature of the liquid phase by about 50 K (°C) and facilitates the formation of an additional liquid, resulting in better densification at 1473 K (1200 °C). In both Fe-B-Cr and Fe-B-Cr-C steels, increasing the chromium content from 1.5 to 3 wt pct raises the temperature of liquid formation by about 10 K (°C). Thermodynamic simulations and experimental results demonstrated that carbon atoms dissolved in austenite facilitate the eutectic reaction and reduce the formation temperature of the liquid phase. In contrast, both chromium and molybdenum atoms dissolved in austenite delay the eutectic reaction. Furthermore, the 3Cr-0.5Mo additive in the Fe-0.4B steel does not change the typical boride structure of M_2B. With the addition of 0.5 wt pct C, the crystal structure is completely transformed from M_2B boride to $M_3(B,C)$ boro-carbide.

DOI: 10.1007/s11661-015-3096-9

I. INTRODUCTION

POWDER metallurgy (PM) steels are widely used to produce automobile and mechanical parts. Their mechanical properties can be improved by adequate microstructures, alloy designs, and processing parameters.[1–9] However, the mechanical performances of PM steels are inferior to those of wrought steels due to their porosity, which ranges from 5 to 15 vol pct. Liquid phase sintering (LPS) is a practical process for decreasing the porosity of PM steels.[10–29] Copper,[26,27] phosphorus,[28,29] and particularly boron[10–25] are effective alloying elements for LPS in PM steels. Boron induces a eutectic reaction ($Fe + Fe_2B \rightarrow L$) and improves the densification. The influence of boron in the LPS of various PM steels, including alloy steels,[10–18] stainless steels,[19–21] maraging steels,[22] and high-Cr steels,[23–25] has been extensively investigated.

Among the material systems of boron-containing PM alloy steels, Fe-B[10–13,18] and Fe-B-Mo[10–14,18] are two major systems investigated. German *et al.*[10] investigated the Fe-(0~1.1 wt pct)B-(0~5 wt pct)Mo steels and found that at a given boron content, increasing the molybdenum concentration leads to the formation of $FeMo_2B_2$ compound and thus reduces the amount of liquid phase. However, Dudrová *et al.*[11] indicated that the LPS densification of Fe-B-1.5Mo steel is better than that of Fe-B, even though the added 1.5 wt pct Mo reduces the amount of liquid phase available at 1473 K (1200 °C). Selecká *et al.*[12] also found that the sintered density after LPS of Fe-0.4B is improved by increasing the molybdenum content from 0 to 1.5 wt pct. Sarasola *et al.*[13] found that the liquid phase forms at 1448 K (1175 °C) in Fe-0.3B steel with molybdenum content lower than 1.5 wt pct. In Fe-0.3B-3.5Mo steel, however, the temperature of eutectic reaction is higher than 1473 K (1200 °C).

The influences of carbon on the LPS of boron-containing PM steels have also been studied.[15–18,22] Xiu *et al.*[17] found that increasing the carbon content from 0.2 wt pct to 0.44 wt pct improves the sintered density of Fe-B-Mo-C steel. Sercombe[22] showed that the onset of the LPS temperature of maraging steel with carbon is ~60 K (°C) lower than that of maraging steel without carbon. The carbon lowers the melting point, so carbon-containing liquids can be formed. In contrast, Liu *et al.*[16] indicated that the effect of carbon on LPS densification is not obvious in Fe-0.3B-1Ni-1Mo-C steel with up to 0.4 wt pct C. Recently, Wu[18] studied the effects of carbon and molybdenum on the LPS of

MING-WEI WU, Associate Professor, and WEN-ZHANG CAI, Master Student, are with the Department of Materials and Mineral Resources Engineering, National Taipei University of Technology, No. 1, Sec. 3, Zhong-Xiao E. Rd., Taipei 10608, Taiwan, ROC. Contact emails: mwwu@ntut.edu.tw; r91527045@ntu.edu.tw YU-CHI FAN, Graduated Master Student, and HER-YUEH HUANG, Associate Professor, are with the Department of Materials Science and Engineering, National Formosa University, No. 64, Wunhua Rd., Huwei, Yunlin 63201, Taiwan, ROC.

Manuscript submitted July 17, 2014.
Article published online August 20, 2015

Fe-0.4B steel using differential scanning calorimetry and thermodynamic simulation. The author found that adding 0.5 wt pct C can facilitate the formation of a secondary liquid phase and increase liquid volume by 5.4 vol pct at 1523 K (1250 °C), thereby improving the sintered density. Adding 1.5 wt pct Mo to Fe-0.4B-0.5C steel can further increase the liquid volume by 1.4 vol pct at 1523 K (1250 °C) and raise the sintered density.

Chromium is also an important alloying element in PM alloy steels due to its high hardenability and low price.[30–32] Lozada and Castro[19] investigated the LPS of three boron-containing PM stainless steels with 11.8, 16.9, and 30 wt pct Cr and showed that increasing the chromium content from 11.8 wt pct to 30 wt pct inhibits LPS. In Fe-30Cr steel, the formation of liquid is completely suppressed, even at temperatures as high as 1648 K (1375 °C). Moreover, according to Selecká *et al.*,[12] the LPS densifications of two chromium-containing steels (Fe-B-1Cr-0.3V-0.3Mo-0.2C and Fe-B-3Cr-0.3V-0.3Mo-0.2C) are greatly inferior to those of Fe-B, Fe-B-2Ni-0.5Mo, Fe-B-0.85Mo, and Fe-B-1.5Mo steels after 1473 K (1200 °C) sintering. The above discoveries clearly show the complexity and importance of various alloying elements in LPS. Unfortunately, only the various stainless steels and high-Cr steels have received much focus. The influences of chromium on the LPS of PM alloy steels have been investigated very little. This study investigated the effects of chromium and carbon on the LPS of boron-containing PM steel. The microstructures and LPS progress of Fe-B-Cr and Fe-B-Cr-C steels were examined and discussed.

II. EXPERIMENTAL PROCEDURE

To clarify the roles of chromium and carbon in the LPS of boron-containing PM alloy steels, Fe-0.4B-1.5Cr, Fe-0.4B-3Cr, Fe-0.4B-1.5Cr-0.5C, and Fe-0.4B-3Cr-0.5C steels were produced and studied. The designations of these four steels were FB-1.5Cr, FB-3Cr, FBC-1.5Cr, and FBC-3Cr, respectively. The base powders were Fe-1.5Cr-0.2Mo (CrL, Höganäs AB, Höganäs, Sweden) and Fe-3Cr-0.5Mo (CrM, Höganäs AB, Höganäs, Sweden) prealloyed powders. The average particle sizes of these two prealloyed powders were approximately 70 μm, according to observations by SEM (JSM-6360, JEOL, Tokyo, Japan). The presence of 0.2 and 0.5 wt pct Mo does not apparently affect the LPS of PM steels because LPS densifications of Fe-B and Fe-B-0.85Mo steels are comparable, as reported by Selecká *et al.*[12] Elemental boron (ELECMAT, CA, USA) and graphite (1651, Asbury Carbons, LA, USA) powders were used to produce the boron-containing PM steels and were investigated in this study. The average particle sizes of the boron and graphite powders were about 2 and 9 μm, respectively. The purities of boron and graphite powders were higher than 99.9 and 95 pct, respectively.

First, the two base powders were blended with 0.4 wt pct elemental boron powder in a mixer for 60 minutes to formulate the FB-1.5Cr, FB-3Cr powder mixtures. To prepare the steels with 0.5 wt pct C, 0.6 wt pct graphite powder was also admixed into the FB-1.5Cr and FB-3Cr powder mixtures. Due to decarburization after sintering, the combined carbon content of FBC-1.5Cr and FBC-3Cr steels was about 0.5 wt pct. Also added to the four powder mixtures was 0.75 wt pct lubricant (ethylene bis-stearamide). Subsequently, these four powder mixtures were uniaxially compacted at a pressure of 600 MPa to prepare green compact disks that were 13 mm in diameter and 7 mm thick. The green densities of these four steels were slightly different due to discrepancies in powder compressibility. The green densities of FB-1.5Cr, FB-3Cr, FBC-1.5Cr, and FBC-3Cr were 6.87, 6.83, 6.84, and 6.81 g/cm^3, respectively. The green densities reported were averages of six specimens. For debinding of the lubricant, the green compacts were heated at 5 K (°C)/min to 823 K (550 °C) and then soaked for 15 minutes. Afterward, the debound specimens were immediately heated at 10 K (°C)/min to the sintering temperatures 1423 K, 1473 K, and 1523 K (1150 °C, 1200 °C, and 1250 °C) without holding, followed by furnace cooling. An atmosphere of argon was used for the debinding and sintering. The debound specimens were also sintered at 1523 K (1250 °C) and held for 1 hour. However, increasing the sintering time to one hour did not apparently affect the results, and the data on 1-hour sintering were thus not included in this study.

The sintered densities of the four steels were measured using the Archimedes method. The metallographic specimens were ground, polished, and etched with a solution of 2 pct Nital and 4 pct Picral, and were finally examined under an optical microscope (OM). An electron probe micro-analyzer (EPMA, JXA-8200SX, JEOL, Tokyo, Japan) was used to measure the distributions of alloying elements and the compositions of borides in the steels, and the crystal structures of borides were determined by a field-emission scanning electron microscope (FE-SEM, Nova NanoSEM 450, FEI, Oregon, USA) equipped with an electron backscatter diffraction (EBSD) system (EDAX Inc.). Kikuchi patterns were collected by a Hikari XP camera and were analyzed with TSL orientation imaging microscopy (OIM) 6.0 software. Thermo-Calc software version 4.1 (Thermo-Calc Software, Stockholm, Sweden) coupled with a TCFE7 database was also utilized to simulate quasi-binary and quasi-ternary phase diagrams to correlate the chromium and carbon with the LPS densification. In addition, differential scanning calorimetry (DSC, STA 449 F3, NETZSCH, Selb, Germany) was applied to identify the temperature of liquid formation during sintering.

III. RESULTS AND DISCUSSION

A. *Microstructure*

The microstructures of the four steels are presented in Figures 1, 2, 3, and 4. The microstructures of FB-1.5Cr and FB-3Cr steels sintered at 1423 K (1150 °C) are not shown because no solidification area could be observed,

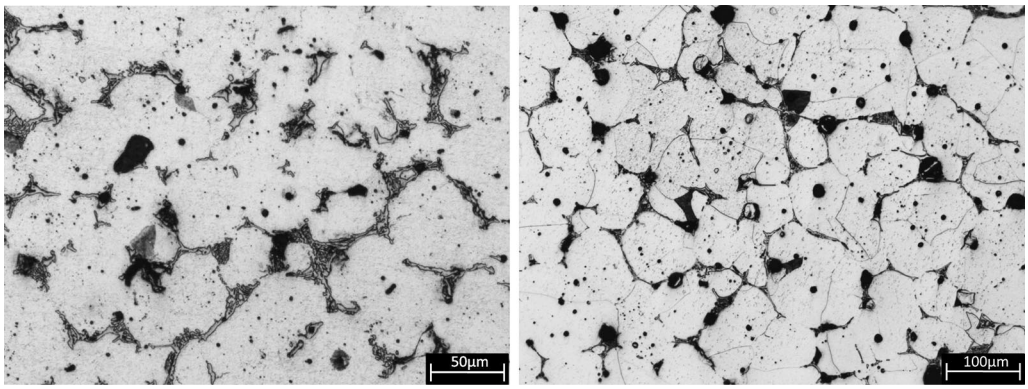

Fig. 1—The microstructures of FB-1.5Cr steels sintered at (*a*) 1473 K (1200 °C) and (*b*) 1523 K (1250 °C).

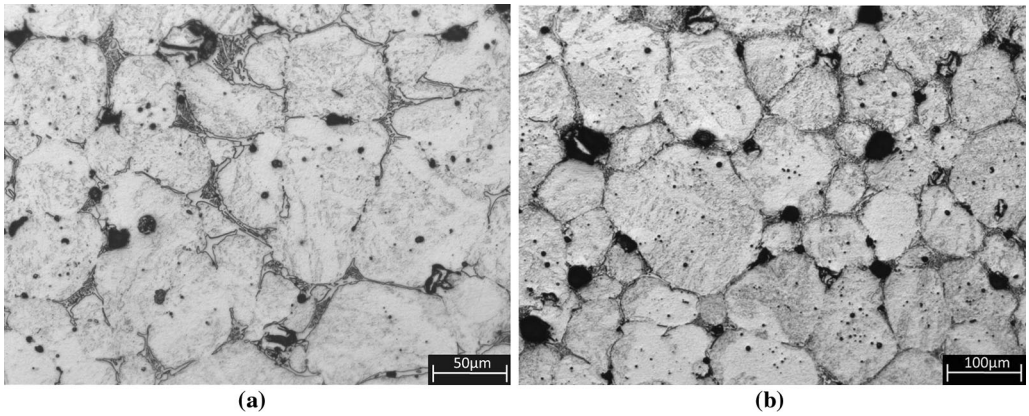

Fig. 2—The microstructures of FB-3Cr steels sintered at (*a*) 1473 K (1200 °C) and (*b*) 1523 K (1250 °C).

indicating that liquid did not form after 1423 K (1150 °C) sintering in the steels without 0.5 wt pct C. In contrast, a few solidification areas could be observed in the steels with 0.5 wt pct C after 1423 K (1150 °C) sintering. When the sintering temperature was increased to 1473 K (1200 °C), eutectic structures or borides could be apparently observed in the four steels, as shown in Figures 1, 2, 3, and 4. Many spherical secondary pores, the original sites of the boron powders, were also found in the microstructure. The microstructures of the four steels sintered at 1473 K (1200 °C) were typical of LPS. However, after 1523 K (1250 °C) sintering, the porosity was only slightly reduced.

After 1423 K (1150 °C) sintering, the microstructures of the FBC-1.5Cr and FBC-3Cr steels at the powder interior were a mixture of pearlite/ferrite and bainite, respectively, implying that most of the carbon atoms diffused into the chromium-containing prealloyed powders from the original graphite powders, as shown in Figures 3(a) and 4(a). The increase in chromium content from 1.5 to 3 wt pct induced the formation of bainite in the interior of the base powder after 1423 K (1150 °C) sintering. Wu[18] reported that minor pearlite was dispersed in the microstructures of Fe-0.4B-0.5C and Fe-0.4B-1.5Mo-0.5C steels, even after 1473 K (1200 °C) sintering. This discrepancy clearly demonstrates that adding chromium can promote the diffusion of carbon atoms into the base powder and thus improve the homogeneity of the carbon. This phenomenon could be attributed to the fact that chromium can effectively decrease the chemical potential of carbon.[7]

B. *Elemental Distribution and Boride Structure*

Figures 5 and 6 show the elemental mappings of FB-3Cr and FBC-3Cr steels sintered at 1523 K (1250 °C), respectively. The findings show that boron, chromium, and molybdenum were mainly concentrated in the borides, irrespective of steel composition. Furthermore, carbon was also concentrated in the borides of FBC-3Cr steel, as shown in Figure 6. It must be noted that a portion of the carbon atoms was distributed in the interior of the base powder due to the presence of carbides, which were too small to observe in Figure 6.

To understand the characteristics of borides in boron-containing PM steels, the compositions of borides in the FB-3Cr and FBC-3Cr steels were also measured using EPMA quantitative analyses, as listed in Table I. The results clearly indicated that the boron contents of the borides in the steels with and without

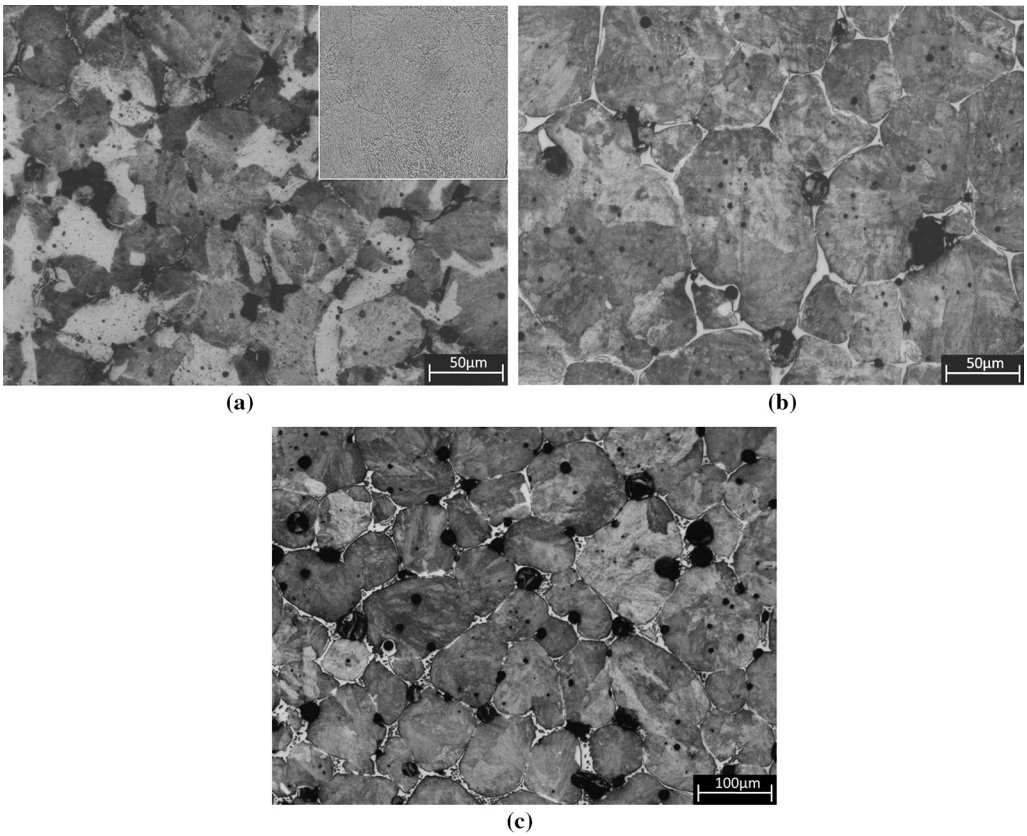

Fig. 3—The microstructures of FBC-1.5Cr steels sintered at (*a*) 1423 K (1150 °C), (*b*) 1473 K (1200 °C), and (*c*) 1523 K (1250 °C).

carbon were significantly divergent. The boron concentration of the borides in FB-3Cr steel was 32.9 at. pct. In the FBC-3Cr steel, the boron and carbon contents of the borides were much lower, 17.5 and 7.8 at. pct, respectively. Surprisingly, the sum of the boron and carbon concentrations in the borides of FBC-3Cr steel was merely 25.3 at. pct. The microstructures of FB-3Cr and FBC-3Cr steels sintered at 1523 K (1250 °C) were also observed using the BSE mode in EPMA, as shown in Figure 7. The contrast between the iron matrix and the boride was obviously greater in FB-3Cr than in FBC-3Cr. The borides in the FB-3Cr steel were darker than those in the FBC-3Cr steel, confirming that more boron atoms were present in the borides of FB-3Cr steel.

The crystal structures of borides in the FB-3Cr and FBC-3Cr steels sintered at 1523 K (1250 °C) were further analyzed using EBSD to identify the influences of carbon on the boride structure. Figures 8 and 9 clearly indicate that the crystal structures of borides in the FB-3Cr and FBC-3Cr steels were M_2B boride and $M_3(B,C)$ boro-carbide, respectively. The atomic ratios of metallic (Fe, Cr, or Mo) and light elements (B or C) in the M_2B and $M_3(B,C)$ structures were 66.7:33.3 and 75:25, respectively. These atomic proportions in the borides of FB-3Cr and FBC-3Cr steels corresponded well to the findings of EPMA quantitative analyses (Table I) and BSE images (Figure 7). In general, the typical boride structure in the boron-containing PM steels was M_2B. EBSD analyses indicated that the 3Cr-0.5Mo additive in the Fe-0.4B steel did not change the M_2B structure. With the addition of 0.5 wt pct C to the FB-3Cr steels, however, the M_2B structure was completely replaced by $M_3(B,C)$.

C. *Thermodynamic Simulation*

To clarify the individual roles of carbon, chromium, and molybdenum on the LPS of boron-containing PM steel, quasi-binary phase diagrams of Fe-0.4B-xC, Fe-0.4B-xCr, and Fe-0.4B-xMo as a function of sintering temperature were simulated using Thermo-Calc software, as shown in Figure 10. The symbols L, γ, M_2B, and Fe_3C in Figure 10 represent liquid, austenite, M_2B boride, and $M_3(B,C)$ boro-carbide, respectively. The simulated results clearly indicated that the addition of carbon in Fe-0.4B could decrease the temperature of eutectic reaction ($\gamma + M_2B \rightarrow L$). In contrast, the temperature of eutectic reaction could be increased by raising the chromium or molybdenum content.

Figure 11 shows the quasi-ternary phase diagrams of Fe-xB-yC and Fe-xB-yC-3Cr-0.5Mo steels at 1523 K (1250 °C). The compositions of FB-3Cr and FBC-3Cr are marked as a solid circle and an open circle, respectively. The simulated phase diagrams indicated that the equilibrium phases of FB-3Cr and FBC-3Cr at 1523 K (1250 °C) were $\gamma + M_2B$ and $L + \gamma + M_2B$,

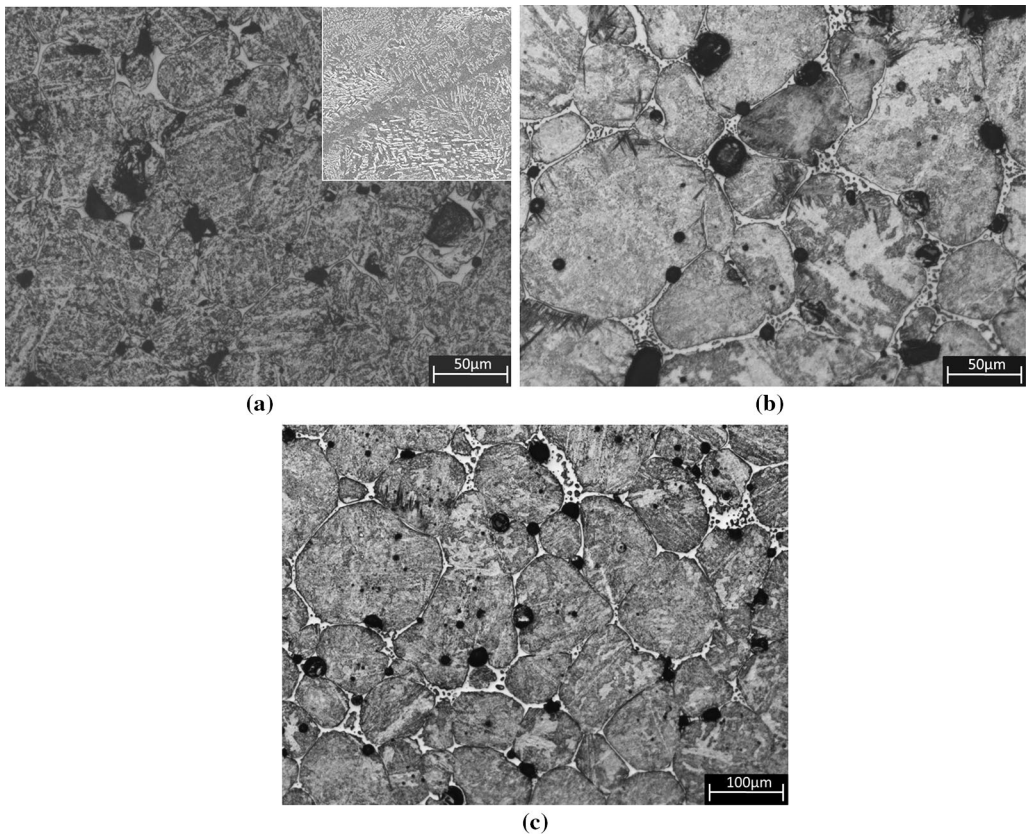

Fig. 4—The microstructures of FBC-3Cr steels sintered at (*a*) 1423 K (1150 °C), (*b*) 1473 K (1200 °C), and (*c*) 1523 K (1250 °C).

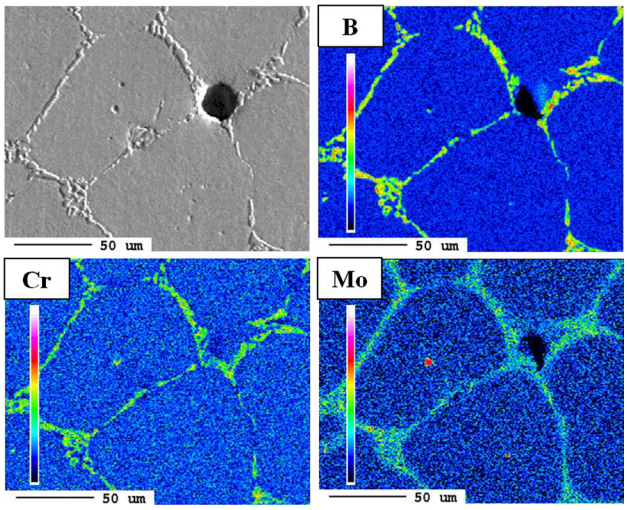

Fig. 5—Elemental mappings of boron, chromium, and molybdenum in the FB-3Cr steel sintered at 1523 K (1250 °C).

respectively, implying that liquid could exist only in the FBC-3Cr steel. To equilibrate with a liquid phase at 1523 K (1250 °C), the boron content in a local region must attain about 1.8 wt pct if there are no carbon atoms in the same region. Furthermore, the presence of carbon reduced the boron content required for liquid formation, as indicated in Figure 11, and *vice versa*. Both boron and carbon atoms participated in the liquid formation.

Nevertheless, the findings on the simulated phase diagrams did not completely match those on the microstructures. Figures 1, 2, 3, and 4 clearly show that liquid formed in the four steels during 1473 K (1200 °C) sintering due to the presence of continuous borides in the microstructure. This discrepancy could be attributed to the PM process and raw powders used in this study. The four steels were prepared by mixing chromium-containing prealloyed powders (70 μm) with elemental boron (2 μm) and graphite (9 μm) powders. The small boron and graphite powders were dispersed in the periphery of chromium-containing base powders after powder mixing, so the boron and carbon were not homogeneously distributed in the powder mixtures or green compacts.

Consequently, the local boron and carbon contents at the periphery of chromium-containing base powders were obviously higher than the nominal concentrations, and these four steels were in a nonequilibrium state during heating and sintering. After sintering, the borides were still mainly concentrated in the boundaries of large Fe-based grains, as displayed in Figures 1, 2, 3, 4, 5, 6, 7, 8, and 9. Since thermodynamic simulation software is utilized to simulate an equilibrium phase diagram, the experimental findings (Figures 1, 2, 3, 4, 5, 6, 7, 8, 9) obtained for a nonequilibrium state did not correspond completely to those calculated with Thermo-Calc software. However, the simulation results (Figures 10 and

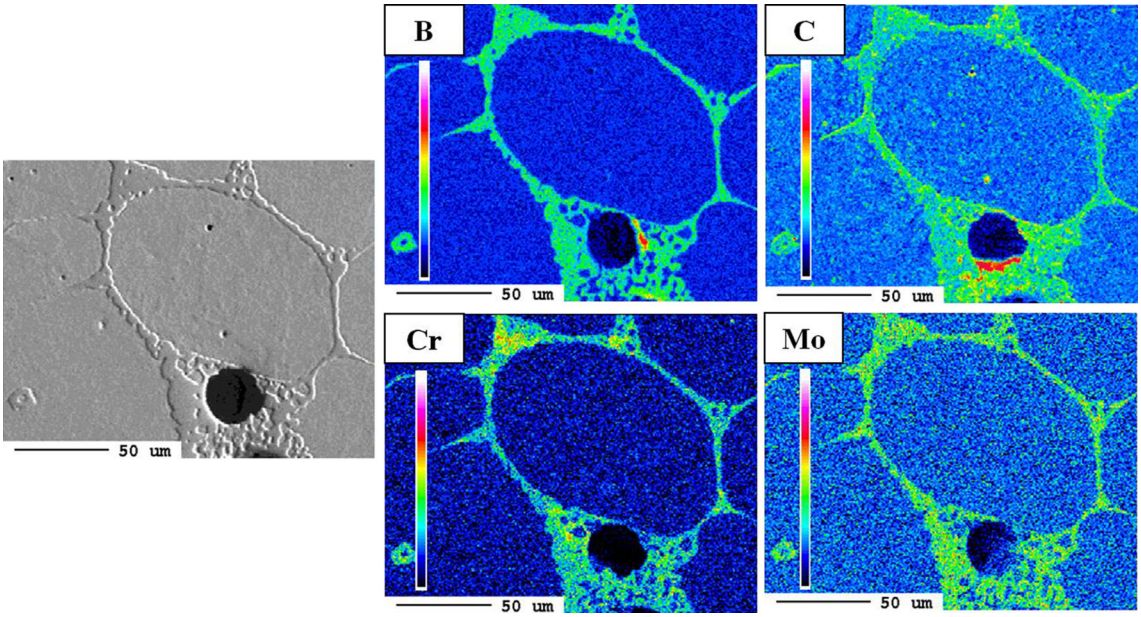

Fig. 6—Elemental mappings of boron, carbon, chromium, and molybdenum in the FBC-3Cr steel sintered at 1523 K (1250 °C).

Table I. The EPMA Quantitative Analyses of the Borides of FB-3Cr and FBC-3Cr Steels Sintered at 1523 K (1250 °C)

Steel Composition	B (at. pct)	C (at. pct)	Cr (at. pct)	Mo (at. pct)	Fe (at. pct)
FB-3Cr	32.86	—	6.66	0.62	Balanced
FBC-3Cr	17.50	7.82	5.74	1.01	Balanced

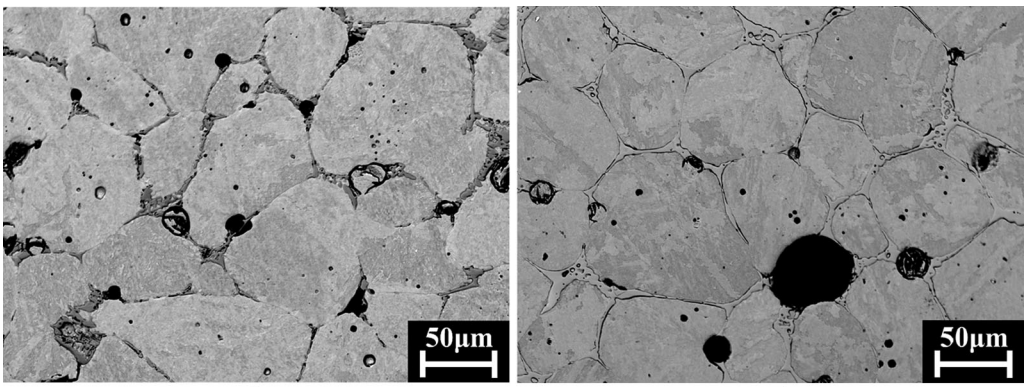

Fig. 7—BSE images of (*a*) FB-3Cr and (*b*) FBC-3Cr steels sintered at 1523 K (1250 °C).

11) did provide information about the roles of carbon, chromium, and molybdenum on the LPS of boron-containing PM steels.

D. *Sintered Density*

The sintered densities at various temperatures and green densities of the four steels are presented in Figure 12. The results indicate that, after 1423 K (1150 °C) sintering, the sintered densities of the steels with 0.5 wt pct C were slightly higher than those of steels without 0.5 wt pct C, even though the trend of green density was reversed. After 1473 K (1200 °C) sintering, the sintered densities of FBC-1.5Cr and FBC-3Cr steels achieved 7.34 and 7.40 g/cm^3, respectively. However, the sintered densities did not significantly change when the sintering temperature was raised from 1473 K to 1523 K (1200 °C to 1250 °C). The final sintered densities of FBC-1.5Cr and FBC-3Cr after 1523 K (1250 °C) sintering were 7.36 and 7.41 g/cm^3, respectively. In contrast, the sintered densities of FB-1.5Cr and FB-3Cr steels were merely about 7.21 and 7.23 g/cm^3, respectively, after 1473 K (1200 °C) sintering. When the sintering temperature was further

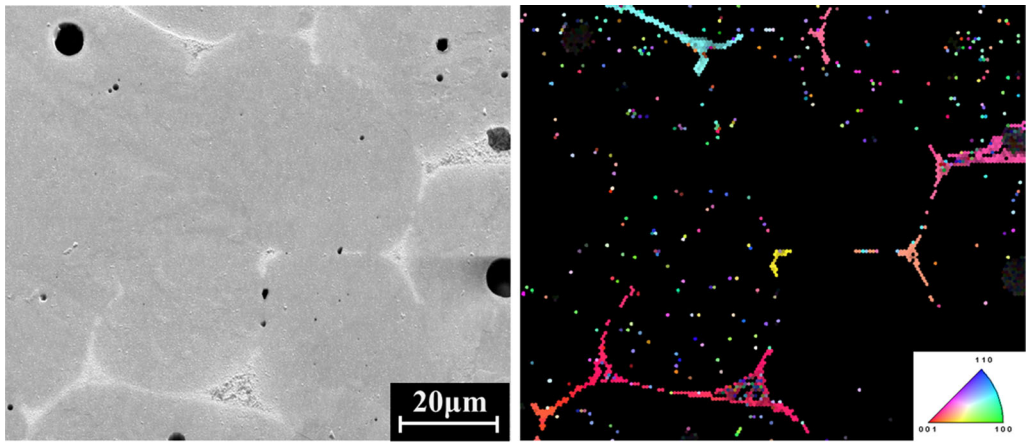

Fig. 8—EBSD analysis of the crystal structure of boride in the FB-3Cr steel. (*a*) Microstructure and (*b*) inverse pole figure of M_2B phase.

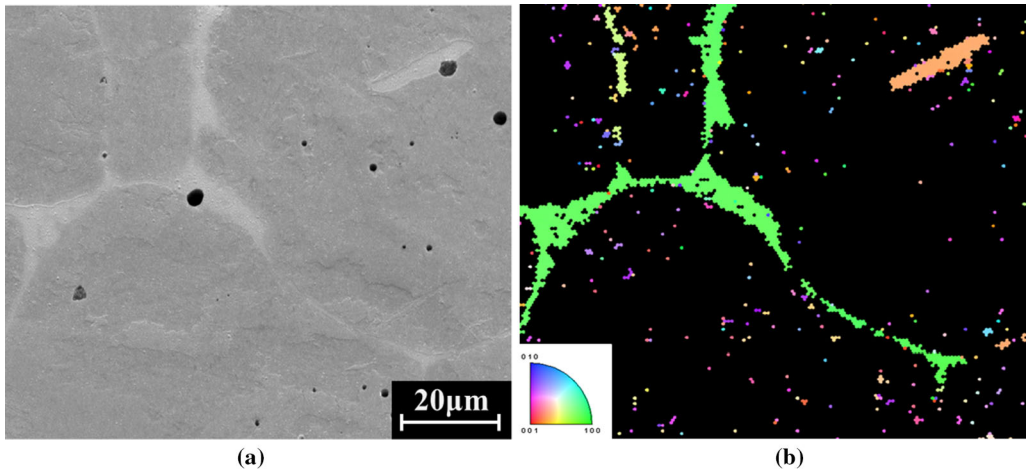

Fig. 9—EBSD analysis of the crystal structure of boride in the FBC-3Cr steel. (*a*) Microstructure and (*b*) inverse pole figure of $M_3(B,C)$ phase.

increased from 1473 K to 1523 K (1200 °C to 1250 °C), the sintered densities of FB-1.5Cr and FB-3Cr were raised to 7.33 and 7.38 g/cm^3, respectively.

The previous findings clearly demonstrate that adding 0.5 wt pct C changes the evolution of LPS in boron-containing PM steels. However, increasing the chromium content from 1.5 to 3 wt pct did not obviously vary the progress of LPS. To exclude the influence of green density on LPS densification, the differences in the sintered densities at 1523 K (1250 °C) and the green densities of the four steels were calculated. The increases in the sintered densities of FB-1.5Cr, FB-3Cr, FBC-1.5Cr, and FBC-3Cr after 1523 K (1250 °C) sintering were 0.46, 0.55, 0.52, and 0.59 g/cm^3, respectively. These results show that 0.5 wt pct C additive slightly increased the sintered density at 1523 K (1250 °C) by about 0.05 g/cm^3, irrespective of the chromium concentration.

E. *Thermal Analysis*

Based on the findings on microstructures, simulated phase diagrams, and sintered densities, it is clear that adding 0.5 wt pct C lowers the temperature of liquid formation. DSC was also used to further clarify the roles of chromium and carbon in the LPS, as shown in Figure 13. In that figure, during LPS of the steels without 0.5 wt pct C, only a single endothermic peak can be observed. The temperature regions for liquid formation in FB-1.5Cr and FB-3Cr were 1453 K~1473 K and 1463 K~1483 K (1180 °C~1200 °C and 1190 °C~1210 °C), respectively. Moreover, a previous study investigating the DSC curve of Fe-0.4B steel also found an endothermic peak between 1443 K and 1458 K (1170 °C and 1185 °C) for liquid formation, which corresponded to the Fe-B eutectic reaction.[18] These results indicate that the formation temperature of liquid phase is raised with increasing the chromium content. This phenomenon could be attributed to the chromium and molybdenum atoms dissolved in austenite, which could stabilize the M_2B boride and delay the eutectic reaction, as shown in Figures 10(b) and (c). Lozada and Castro[19] also found endothermal peaks at around 1493 K and 1513 K (1220 °C and 1240 °C) for the 409 (11.8 wt pct Cr) and 316 (16.9 wt pct Cr-13 wt pct Ni) PM stainless steels, respectively. In Fe-30Cr steel, the

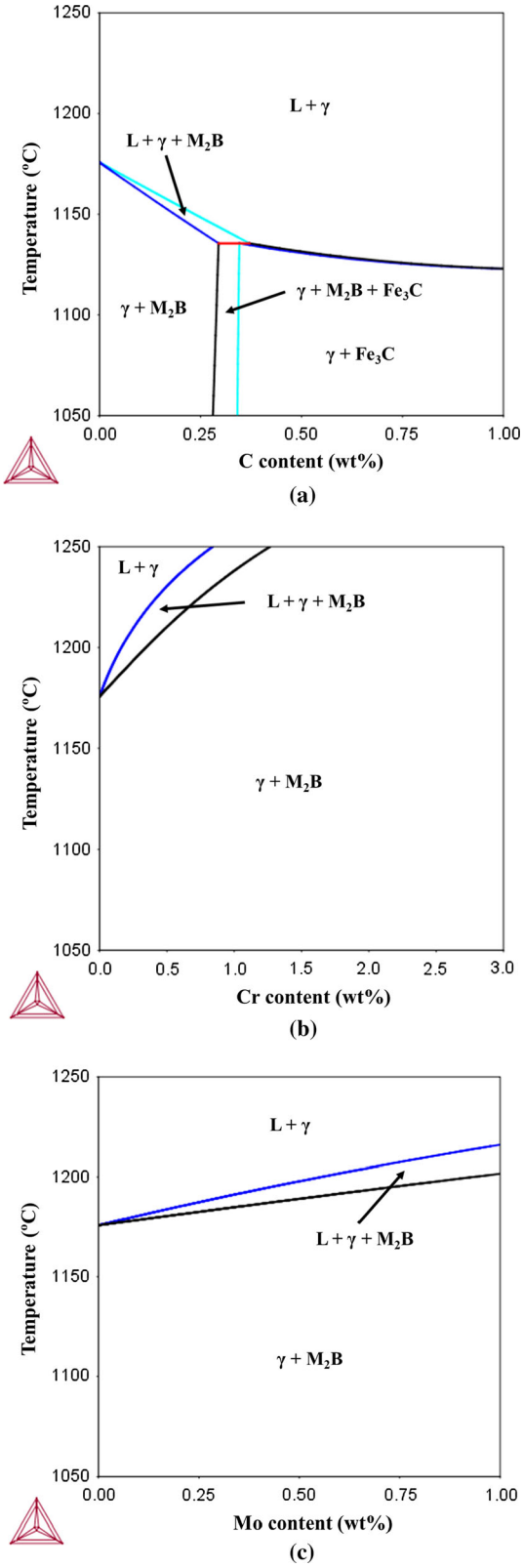

Fig. 10—Simulated quasi-binary phase diagrams of (*a*) Fe-0.4B-xC, (*b*) Fe-0.4B-xCr, and (*c*) Fe-0.4B-xMo steels as a function of sintering temperature.

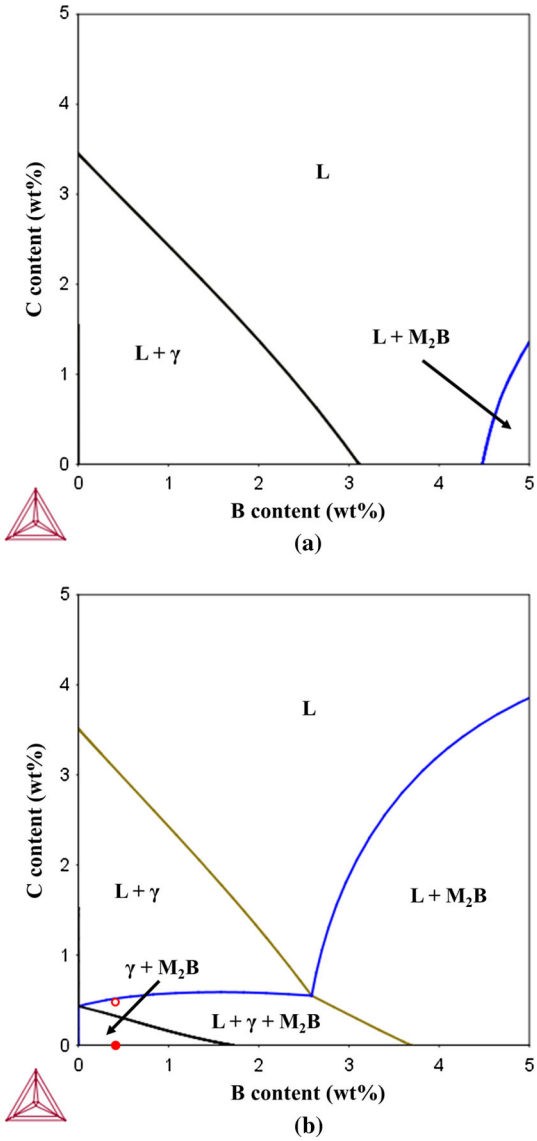

Fig. 11—Simulated quasi-ternary phase diagrams of (*a*) Fe-xB-yC and (*b*) Fe-xB-yC-3Cr-0.5Mo steels at 1523 K (1250 °C).

formation of liquid is completely inhibited even at temperatures as high as 1648 K (1375 °C).

In contrast, two distinct endothermic peaks during LPS of the steels with 0.5 wt pct C can be clearly discriminated in Figure 13(b), though the two peaks are slightly overlapped. The temperature regions for liquid formation of FBC-1.5Cr and FBC-3Cr were 1403 K~1448 K and 1413 K~1458 K (1130 °C~1175 °C and 1140 °C~1185 °C), respectively. The DSC results indicate that adding 0.5 wt pct C reduced the formation temperature of liquid phase by ~50 K (°C). These DSC findings explain why the sintered densities of the steels with 0.5 wt pct C were higher than those without 0.5 wt pct C after 1473 K (1200 °C) sintering, as shown in Figure 12. Selecká *et al.*[12] reported that the LPS densifications of

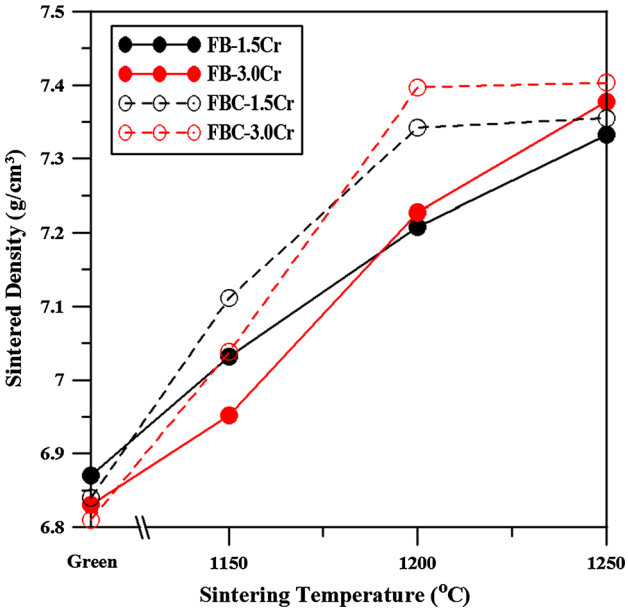

Fig. 12—The sintered densities of the four steels as a function of sintering temperature.

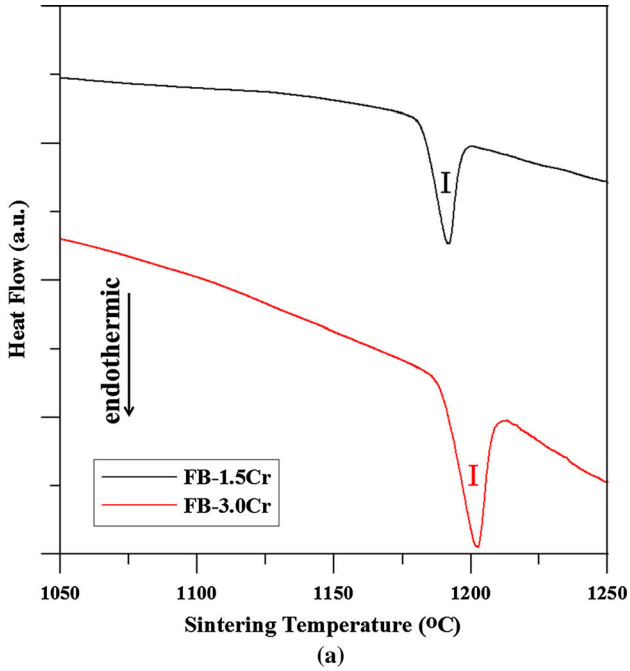

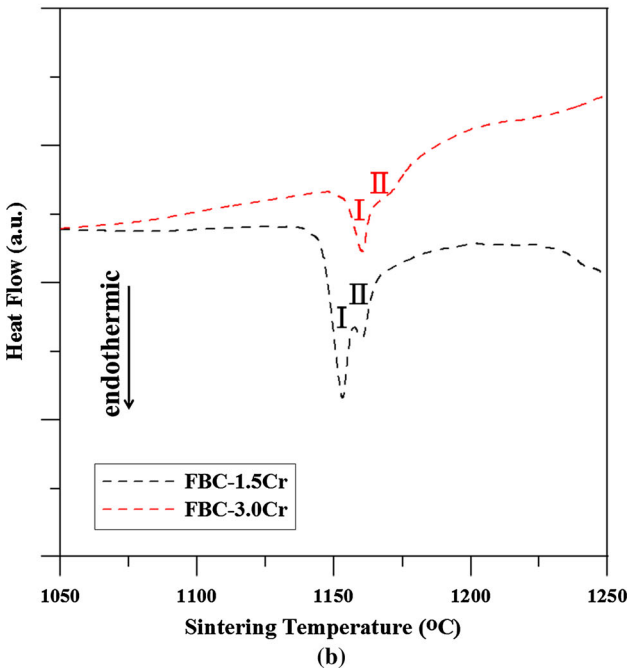

Fig. 13—The heating regions of DSC curves for (*a*) the steels without 0.5 wt pct C and (*b*) the steels with 0.5 wt pct C, as a function of sintering temperature.

two low-Cr steels (Fe-B-1Cr-0.3V-0.3Mo-0.2C and Fe-B-3Cr-0.3V-0.3Mo-0.2C) were far inferior to those of steels without Cr after 1473 K (1200 °C) sintering. Based on the findings in this study, it appears that the inferior LPS densification of Fe-B-1Cr-0.3V-0.3Mo-0.2C and Fe-B-3Cr-0.3V-0.3Mo-0.2C at 1473 K (1200 °C) could be due mainly to the lower sintering temperature and carbon content.

In Section III–C, the simulated quasi-binary phase diagrams of Fe-0.4B-xC indicate that increasing the carbon content in austenite could lower the temperature of eutectic reaction, as shown in Figure 10(a). In the FBC-1.5Cr and FBC-3Cr steels, most carbon atoms diffuse into austenite during 1423 K (1150 °C) sintering, and pearlite or bainite was extensively observed in the microstructure, as shown in Figures 3(a) and 4(a). Moreover, the 0.5wt pct C additive in FB-3Cr steel changed the boride structure from M_2B to $M_3(B,C)$, indicating that carbon atoms participated in the liquid formation. Thus, the carbon atoms dissolved in austenite facilitated the eutectic reaction and reduced the formation temperature of the liquid phase.

Furthermore, in the FBC-1.5Cr and FBC-3Cr steels, liquid was formed at two temperature regions. In a previous study, secondary liquid was also observed in Fe-0.4B-0.5C and Fe-0.4B-1.5Mo-0.5C steels.[18] To understand the formation of secondary liquid in the steels with 0.5 wt pct C, the microstructure of FBC-3Cr steel sintered at 1418 K (1145 °C) was also examined in detail. Figure 14 shows that two kinds of borides, M_2B and $M_3(B,C)$, were present in the FBC-3Cr steel sintered at 1418 K (1145 °C), and the morphologies of those two borides were obviously different. The M_2B boride was granular or blocky in shape. In contrast, the $M_3(B,C)$ boro-carbide was strip-like in shape and was mostly dispersed at the grain boundary. These findings show that the $M_3(B,C)$ boro-carbide originated from a liquid, which was generated during sintering at 1418 K (1145 °C). At a higher temperature, the M_2B boride could react with austenite to form a secondary liquid. In conclusion, this study clearly demonstrates that adding 0.5 wt pct C in Fe-B-Cr alloy steels decreases the temperature of liquid formation and facilitates the generation of secondary liquid, resulting in better LPS densification at lower sintering temperature.

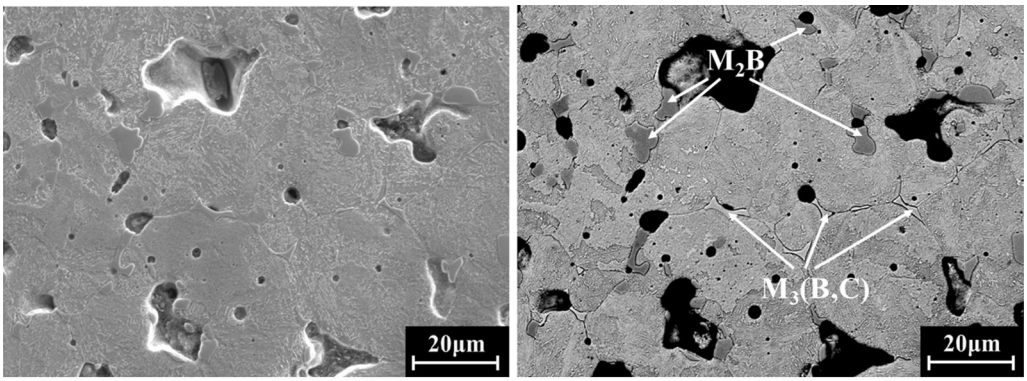

Fig. 14—The microstructure of FBC-3Cr steel sintered at 1418 K (1145 °C). (*a*) SE image and (*b*) BSE image.

IV. CONCLUSIONS

This study identified the effects of chromium and carbon on the microstructure, elemental distribution, boride structure, sintered density, and liquid formation of Fe-B-Cr and Fe-B-Cr-C steels during LPS. The findings are summarized as follows.

1. During 1423 K (1150 °C) sintering, liquid forms only in the steels with 0.5 wt pct C. No solidification area can be found in steels without 0.5 wt pct C. When the sintering temperature is increased to 1473 K (1200 °C), a large amount of liquid can be generated in steels with and without 0.5 wt pct C.
2. The crystal structures of borides in the FB-3Cr and FBC-3Cr steels are M_2B and $M_3(B,C)$, respectively. The boron, chromium, and molybdenum predominantly concentrate in the areas of borides. In the steels with 0.5 wt pct C, carbon atoms are distributed in not only the carbides but also the boro-carbides.
3. Increasing the chromium content from 1.5 wt pct to 3 wt pct raises the formation temperature of the liquid phase by about 10 K (°C) in the Fe-B-Cr and Fe-B-Cr-C steels.
4. During LPS, only one liquid phase forms in Fe-B-Cr steels. Adding 0.5 wt pct C to Fe-B-Cr steels greatly reduces the formation temperature of the liquid phase by about 50 K (°C), and a secondary liquid is generated, resulting in better LPS densification at 1473 K (1200 °C).
5. Thermodynamic simulations and experimental results showed that both boron and carbon atoms participate in liquid formation. Furthermore, the above analyses also demonstrated that both chromium and molybdenum atoms dissolved in austenite delay the eutectic reaction and liquid formation. In contrast, carbon atoms dissolved in austenite facilitate the eutectic reaction and reduce the formation temperature of the liquid phase.

ACKNOWLEDGMENT

The authors thank the Ministry of Science and Technology of the Republic of China for supports under Contract Number MOST 103-2221-E-027-132.

REFERENCES

1. J.M. Torralba, A. Navarro, and M. Campos: *Mater. Sci. Eng. A*, 2013, vol. 573, pp. 253–56.
2. H. Danninger, C. Xu, G. Khatibi, B. Weiss, and B. Lindqvist: *Powder Metall.*, 2012, vol. 55, pp. 378–87.
3. J. Desbiens, E. Robert-Perron, C. Blais, and F. Chagnon: *Mater. Sci. Eng. A*, 2012, vol. 546, pp. 218–22.
4. M. Campos, J. Sicre-Artalejo, J.J. Munoz, and J.M. Torralba: *Metall. Mater. Trans. A*, 2010, vol. 41A, pp. 1847–54.
5. F. Bernier, P. Plamondon, J.P. Baïlon, and G. L'Espèrance: *Powder Metall.*, 2011, vol. 54, pp. 559–65.
6. M. Gauthier, S. Metcalfe, S. Pelletier, and T.F. Stephenson: *Powder Metall.*, 2011, vol. 54, pp. 628–35.
7. M.W. Wu, K.S. Hwang, and H.S. Huang: *Metall. Mater. Trans. A*, 2007, vol. 38A, pp. 1598–1607.
8. M.W. Wu, L.C. Tsao, G.J. Shu, and B.H. Lin: *Mater. Sci. Eng. A*, 2012, vol. 538, pp. 135–44.
9. M.W. Wu, G.J. Shu, S.Y. Chang, and B.H. Lin: *Metall. Mater. Trans. A*, 2014, vol. 45A, pp. 3866–75.
10. R.M. German, K.S. Hwang, and D.S. Madan: *Powder Metall. Int.*, 1987, vol. 19, pp. 15–18.
11. E. Dudrová, M. Selecká, R. Bureś, and M. Kabátová: *ISIJ Int.*, 1997, vol. 37, pp. 59–64.
12. M. Selecká, A. Šalak, and H. Danninger: *J. Mater. Process. Technol.*, 2003, vols. 143–144, pp. 910–15.
13. M. Sarasola, T.G. Acebo, and F. Castro: *Acta Mater.*, 2004, vol. 52, pp. 4615–22.
14. A. Molinari, T. Pieczonka, J. Kazior, S. Gialanella, and G. Straffelini: *Metall. Mater. Trans. A*, 2000, vol. 31A, pp. 1497–1506.
15. M. Momeni, C. Gierl, H. Danninger, and A. Avakemian: *Powder Metall.*, 2012, vol. 55, pp. 54–64.
16. J. Liu, A. Cardamone, T. Potter, R.M. German, and F.J. Semel: *Powder Metall.*, 2000, vol. 43, pp. 57–61.
17. Z. Xiu, A. Salwen, X. Qin, F. He, and X. Sun: *Powder Metall.*, 2003, vol. 46, pp. 171–74.
18. M.W. Wu: *Metall. Mater. Trans. A*, 2015, vol. 46A, pp. 467–75.

19. L. Lozada and F. Castro: *Adv. Powder Metall. Part. Mater.*, 2011, Part 7, pp. 78–88.
20. C. Menapace, A. Molinari, J. Kazior, and T. Pieczonka: *Powder Metall.*, 2007, vol. 50, pp. 326–35.
21. H.Ö. Gulsoy: *Scripta Mater.*, 2005, vol. 52, pp. 187–92.
22. T.B. Sercombe: *Mater. Sci. Eng. A*, 2003, vol. 344, pp. 312–17.
23. T.B. Sercombe and G.B. Schaffer: *Mater. Sci. Eng. A*, 2010, vol. 528, pp. 751–55.
24. A. Röttger, S. Weber, and W. Theisen: *Mater. Sci. Eng. A*, 2012, vol. 532, pp. 511–21.
25. G. Cui and Z. Kou: *J. Alloys Compd.*, 2014, vol. 586, pp. 699–702.
26. R.L. Lawcock and T.J. Davies: *Powder Metall.*, 1990, vol. 33, pp. 147–50.
27. C.T. Huang and K.S. Hwang: *Powder Metall.*, 1996, vol. 39, pp. 119–23.
28. A. Molinari, G. Straffelini, V. Fontanari, and R. Canteri: *Powder Metall.*, 1992, vol. 35, pp. 285–91.
29. G. Straffelini, V. Fontanari, A. Molinari, and B. Tesi: *Powder Metall.*, 1993, vol. 36, pp. 135–41.
30. S. Bueno, S. Saccarola, A. Karuppannagounder, A. Veiga, S. Sainz, and F. Castro: *Powder Metall.*, 2012, vol. 55, pp. 92–94.
31. N. Giguère and C. Blais: *Metall. Mater. Trans. A*, 2013, vol. 44A, pp. 4774–87.
32. L. Čiripová, E. Hryha, E. Dudrová, and A. Výrostková: *Mater. Des.*, 2012, vol. 35, pp. 619–25.